Sizing of Bovine Heart and Kidney Pyruvate Dehydrogenase Complex and Dihydrolipoyl Transacetylase Core by Quasielastic Light Scattering†

T. E. Roche,*,‡ S. L. Powers-Greenwood,‡ W. F. Shi,§ W. B. Zhang,§ S. Z. Ren,§ E. D. Roche,‡ D. J. Cox,‡,∥ and C. M. Sorensen§

Departments of Biochemistry and Physics, Kansas State University, Manhattan, Kansas 66506

Received December 29, 1992; Revised Manuscript Received March 15, 1993

ABSTRACT: Quasielastic light scattering (QELS) measurements on several preparations of bovine heart and kidney pyruvate dehydrogenase complex yielded hydrodynamic radii (r_H values) ranging from 25.7 to 30 nm. Gel filtration chromatography removed stable aggregates and generated preparations that gave essentially the same r_H values of 24.3 ± 0.6 nm for both complexes. The data were characteristic of a monodisperse system and agree with estimates using cryoelectron microscopy [Wagenknecht et al. (1991) *J. Biol. Chem. 266*, 24650–24656]. The equivalent hydrodynamic sizes for the heart and kidney complex indicate that the larger number of pyruvate dehydrogenase components in the heart complex ($M_r \simeq 9 \times 10^6$) than the kidney complex ($M_r \simeq 7.5 \times 10^6$) associate without radial expansion of the heart complex. That accommodation of additional mass is consistent with the space available since even in the more massive complex greater than 80% of the volume within the dimensions of the complex must be occupied by solvent. Preparations of the core of the complex are primarily composed of 60 dihydrolipoyl acetyltransferase (E2) subunits whose inner domains associate to form a pentagonal dodecahedron that is readily observed by electron microscopy (particle radius 10.7–11.3 nm). However, the bulk of E2's mass is present in an exterior multidomain structure. These mobile outer structures are very difficult to observe by standard electron microscopy techniques. Preparations of the core formed stable aggregates that were removed by gel filtration chromatography. QELS measurements gave an r_H of 20.1 ± 0.8 nm. Thus, while occupying only a small fraction of the volume exterior to the inner core, the outer domains must contribute significant hydrodynamic drag to give an ~9 nm increase in r_H beyond the radius of the structurally symmetric inner core. The binding of other components to form the heart complex more than triples the protein mass exterior to the core while adding only 3.5–5 nm to r_H.

The pyruvate dehydrogenase complex has a central and strategic role in metabolism. In mammalian cells, the activity of this multienzyme complex is modulated by an intricate phosphorylation–dephosphorylation cycle that responds to both intrinsic and extrinsic control. The size and structural organization of this giant enzyme complex has been pursued by several techniques. Major insights into the organization of this supramolecular assemblage came from negative stain electron microscopy (Reed & Oliver, 1968; Oliver & Reed, 1982). Key to the arrangement of component enzyme molecules in the complex is the structure and organization of the dihydrolipoyl transacetylase (E2)[1] subunits that form the core of the complex. This apparently symmetric assemblage of subunits is proposed to have rotational 5:3:2 (icosahedral) symmetry and to be composed of 60 E2 subunits with three subunits at each of the 20 vertices of the polyhedron. In electron micrographs the inner core of the complex has the appearance of a pentagonal dodecahedron (Reed & Oliver, 1968). Another lipoyl-bearing subunit, protein X, is tightly bound to this framework (Rahmatullah et al., 1989a; Patel & Roche, 1990). Protein X is present at about one-tenth the level of E2 subunits (Jilka et al., 1986). The other components, both regulatory and cardinal components for the overall reaction, bind to the E2–X subcomplex. In the case of the bovine heart pyruvate dehydrogenase complex, the M_r of the isolated complex (lacking the pyruvate dehydrogenase phosphatase but containing all the other components) is about 9.0×10^6. Resolution of the complex yields an E2–X preparation that retains about two pyruvate dehydrogenase kinase heterodimers (K_cK_b subunits). This E2–X–K_cK_b subcomplex has an M_r of about 4.0×10^6.

Both the E2 and protein X have structures consisting of an aggregate forming inner domain and of a multidomain outer structure (Bleile et al., 1981; Rahmatullah et al., 1989a; Coppel et al., 1988; Thekkumkara et al., 1988). The inner domains of E2 subunits form the dodecahedron structure observed in electron micrographs. Recently, the structure of the octohedron forming inner domain of *Azotobacter vinelandii* has been determined to 2.6-Å resolution (Mattevic et al., 1992). Their work established that the dimensions determined for the cubic-shaped inner core structure by electron microscopy are accurate within 10%. We will assume ice-imbedded electron (cryoelectron) microscopy measurements (Wagenknecht et al., 1991b) on the rigid dodecahedron inner core of[2]

† This work was supported by U.S. Public Health Service Grant DK18320 and by Kansas State Agriculture Experiment Station Contribution 91-559-J.

* To whom correspondence should be addressed.
‡ Department of Biochemistry.
§ Department of Physics.
∥ Current address: Indiana University–Purdue University at Ft. Wayne.

[1] Abbreviations: PDC, pyruvate dehydrogenase complex; E1, pyruvate dehydrogenase component; E2, dihydrolipoyl transacetylase component; $E2_L$, fragment of E2 containing both lipoyl domains; X, protein X; K_c, catalytic subunit of the kinase; K_b, basic subunit of the kinase; E3, dihydrolipoyl dehydrogenase; QELS, quasielastic light scattering; PMT, photomultiplier tube.

[2] A 3-D reconstruction of the dodecahedron-shaped inner core of mammalian E2 has been developed from cryoelectron micrographs to about 22-Å resolution (V. V. P. Prasad, T. Wagenknecht, and T. E. Roche, manuscript in preparation). This agrees with the measurements reported by Wagenknecht et al. (1991) for the size of the inner core of the mammalian complex.

0006-2960/93/0432-5629$04.00/0

mammalian E2 (diameter in 5-fold orientation was 22.5 nm) are similarly accurate.[2] Of particular interest, from the high-resolution structure of Mattevic et al. (1992) was the discovery that, for catalysis of the transacetylation reaction by the active site of inner domain of the *A. vinelandii* E2, CoA must enter the active site from the interior of the oligomeric structure. Thus, this gives a role for the water space within the cubic and dodecahedron inner core structures. The present work will emphasize the large water space encompassed within the E2 structure exterior to the inner core.

More than half of the mass of mammalian E2 is present in its multidomain structure exterior to the inner core. However, this portion of the structure is not resolved in cryoelectron microscopy, and outer domains were poorly contrasted irregularly positioned zones extending for an indefinite distance (at least 5 nm) from the inner dodecahedron structure in negatively stained images (Bleile et al., 1981). When, in the negative stain procedures, the molecules are dried on micrograph grids, the mobile outer domains may contract and form artificial aggregates that contribute most of the contrast observed in electron micrographs. In solution these anionic outer domains would be expected to project in a more uniform and possibly more extended fashion.

The outer domain of E2 subunits comprises three subdomains connected by flexible intersubdomain segments (hinge or linker regions) (Coppel et al., 1988; Thekkumkara et al., 1988). Two NH_2-terminal subdomains are related lipoyl-bearing regions. The third subdomain functions in the binding of the pyruvate dehydrogenase (E1) component (Rahmatullah et al., 1989b, 1990). A 28-kDa $E2_L$ fragment containing both lipoyl domains and the successive hinge region can be selectively released by collagenase treatment of E2 (Rahmatullah et al., 1990) leaving the E1-binding domain attached to the inner oligomeric structure. The lipoyl domains of E2 and of protein X (Rahmatullah et al., 1990) move between multiple active sites to make the dithiolane ring of the lipoyl moiety available for three different reactions within the complex.

Intact complexes (bacterial and mammalian), assembled E2 subcomplexes, and the proteolytically released lipoyl domains exhibit a high (>1.8) frictional ratios (f/f_o).[3] Cryoelectron microscopy has indicated that the mammalian complex (Wagenknecht et al., 1991) as well as *Escherichia coli* complex have tethered E1 and E3 components (i.e., gaps between the bound components and inner core). That is consistent with a large water shell contributing to the high frictional drag of these nearly spherical structures (cf. Discussion).

In the present work we have used quasielastic light scattering (QELS) (Berne & Pecora, 1976; Bloomfield, 1985) to measure in solution the hydrodynamic diameters of the bovine heart and kidney pyruvate dehydrogenase complexes, the assembled E2–X–K_cK_b subcomplex, and the $E2_L$ fragment. The kidney complex contains less E1 and has an M_r about 1 500 000 below that of the heart complex (Reed, 1974). A serious difficulty encountered was the effect of low levels of aggregates in the preparations of E2–X–K_cK_b subcomplex and isolated lipoyl domains. This difficulty was overcome by making measurements immediately following isolation of the nonaggregated structures by gel filtration chromatography. Trace levels of aggregates were also removed from preparations of the bovine heart and kidney complexes. Our measurements allow an estimate of the minimal extension of the outer domains of the assembled core (cf. Discussion) and define the relationship between the hydrodynamic diameter of the E2–X–K_cK_b subcomplex and the entire complex. We have found that the intact complex and the E2–X–K_cK_b subcomplex have larger hydrodynamic diameters than would be predicted from electron microscopy of negatively stained images (Bleile et al., 1981) and somewhat larger than values determined for glutaraldehyde cross-linked particles using two-dimensional agarose gel electrophoresis (Easom et al., 1989). Our measurements of the size of the bovine kidney and heart pyruvate dehydrogenase complexes are in close agreement with measurements using cryoelectron microscopy (Wagenknecht et al., 1991b).

EXPERIMENTAL PROCEDURES

Enzymes. Standard procedures were used to prepare bovine heart and kidney pyruvate dehydrogenase complexes (Roche & Cate, 1977), E2–X–K_cK_b subcomplex (Linn et al., 1972), and collagenase-generated $E2_L$ fragment (Rahmatullah et al., 1990b). Aggregates were removed from preparations by gel filtration chromatography with a 60 × 0.7 cm Sephacryl S-400 column (complexes and subcomplex) or similarly sized Sephacryl S-300 column for the $E2_L$ fragment. To remove dust particles, all buffers were passed through 0.45 μm nitrocellulose Millipore filters, all containers and pipette tips were thoroughly rinsed with filtered water and buffer, and containers were immediately sealed after transfers. Just prior to transfer to the cuvette for light scattering measurements, all protein samples were centrifuged at 14 000 rpm for 3 min in Eppendorf 3200 microfuge. About 0.3 mL at the bottom of this tube was not transferred to the curvette.

Quasielastic Light Scattering Approach. The dynamic light scattering apparatus (Olivier & Sorensen, 1990) used an argon ion laser operating at λ = 5145 Å for the incident light source. The vertically polarized beam was focused with a 15-cm focal length lens into a 1-cm square spectrophotometer cuvette which served as the sample cell. The scattered light was collected at one of a variety of possible scattering angles by a 6-cm focal length lens. This lens formed a real image of the scattering volume in the cuvette onto an adjustable iris diaphragm at approximately unity magnification. This allowed for elimination of stray light from cell surfaces, etc., and ensured we were in the homodyne mode of detection. After passing through the iris, the scattered light traveled 0.5 m to the cathode of an ITT FW130 photomultiplier tube (PMT). This long path allowed for the creation of reasonable transverse spatial coherence on the PMT cathode, necessary for good signal-to-noise in the spectrum. Photopulses from the PMT were then amplified, discriminated and shaped, and fed to either one of two commercial correlators which computed the

[3] Beyond the high frictional coefficients [e.g., Danson et al. (1979) for *E. coli* complex and Bleile et al. (1981) for trypsin-generated lipoyl domain fragment of mammalian E2], one can use a combination of sedimentation velocity and sedimentation equilibrium studies to calculate a diffusion coefficient and r_H value. For the bovine heart and the bovine kidney complexes, $S^o_{20,w}$ values were reported to be 90 S and 70 S, respectively (Linn et al., 1972), and M_r values were found by sedimentation equilibrium experiments to be 9×10^6, and 7×10^6, respectively (Reed, 1974). From $D_{20,w} = RT(S^o_{20,w}M_r(1 - v\rho_{20,w})$ and eq 3, an r_H = 23.0 nm is calculated for both complexes. Our best estimate of M_r of our kidney preparations is 7.5×10^6 based on the assumption that there are 60 E2 subunits and of studies to estimate the level of each of the other components: E1, Cate et al. (1979); E3, Wu and Reed (1984); and kinase, Rahmatuallah et al. (1987); protein X, Jilka et al. (1986). Our preparations of kidney complex give an $S^o_{20,w}$ of 73. Those numbers yield an r_H of 23.6 nm. Both rounding of the first set of numbers (no error information indicated) and limitations in our estimates of subunit composition could introduce substantial errors. It is encouraging that these values are within 5% the values determined herein by QELS.

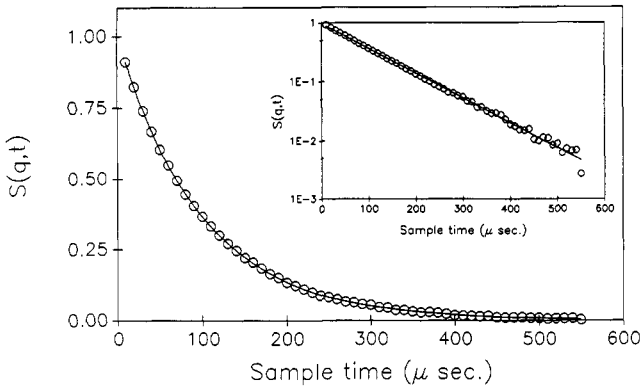

FIGURE 1: Normalized correlation function $S(q,t)$ for light scattering at an angle of 90° and temperature of 22.8 °C for a sample of kidney pyruvate dehydrogenase complex prepared by gel filtration chromatography in 0.05 M Na MOPS (pH 7.4). The sample time in each channel was 10 μs. The cumulant ratio ≅ 0.02. This measurement gave a τ_c of 1.04×10^{-4} s and a particle diameter of 49.3 nm. The average of several such measurements on a similar sample gave a 1% smaller diameter (data Figure 3). The inset is a semilog plot of the data and shows the linear fit predicted for a well-behaved exponential.

intensity–intensity autocorrelation function of the scattered light. Typical input laser powers of ~10 mW allowed for accumulation of clean spectra in roughly 1 min run times.

During the early part of this work a Langley-Ford Model 1 correlator was used. This correlator has 64 equally spaced channels with variable sample time per channel. Analysis of the data was performed in an on-line computer using the method of cumulants. In this fit method the intensity auto correlation function is writen as

$$\langle I(0)I(t)\rangle = B + Ae^{-\mu_1 t+(1/2)\mu_2 t^2} \quad (1)$$

In eq 1, B is the background determined from either the photocount statistics available in the correlator or from the average of eight channels which can be automatically delayed to long t. These values typically agreed to better than 1%, and the agreement was used as an indicator of a successful run. A is the signal amplitude, and typically $A/B \simeq 0.3$. These data were fit by calculating the normalized correlation function, i.e., the dynamic structure factor as $S(q,t) = [\langle I(0)I(t)\rangle - B]/A$, defined so that $S(q,0) = 1$ and $S(q,\infty) = 0$. The cumulants are μ_1 and μ_2, and in the one cumulant fit, μ_2 was set to zero. μ_1 is the key size determining factor and is equal to the inverse of the correlation time, τ_c^{-1}, of the scattered light. Typical results for our data are shown in Figure 1.

The cumulants yield mean size and size distribution information. In the homodyne detection mode, the first cumulant is given by

$$\mu_1 = \tau_c^{-1} = 2Dq^2 \quad (2)$$

Here D is the particle diffusion coefficient,

$$D = \frac{k_B T}{6\pi\eta r_H} \quad (3)$$

where k_B is Boltzmann's constant, T is the absolute temperature, η is the viscosity of the liquid medium, and r_H is the mean hydrodynamic particle radius. Also in eq 2 is the scattering wave vector

$$q = 4\pi n\lambda^{-1} \sin\frac{\theta}{2} \quad (4)$$

where n is the liquid medium index of refraction, $\lambda = 5145$ Å is the optical wavelength, and θ is the scattering angle.

During the course of our work, a second correlator was obtained; an ALV 5000 with Transputer Board. This state-of-the-art device has 256 logarithmically spaced channels. The Transputer Board allows for analysis of the scattered light autocorrelation function with either the two-cumulant method, similar to that described above, or the CONTIN procedure of Provencher (1982). This fit determines a correlation time distribution which best describes the autocorrelation function. The data obtained and analyzed with this new correlator were, within experimental precision, completely consistent with those obtained with the older Langley-Ford.

An important criterion for the efficacy of our correlation data is in the q^2 dependence of the correlation time. Hence a check of the q^2 dependence was made by varying θ for a given sample. A graph of log τ_c versus log q should be linear with a slope of 2. Some samples showed q^x dependencies with $3 > x > 2$. This is an indication of power law polydispersity, i.e., the size distribution $N(r) \sim r^{-z}$, where z is some power (Martin & Leyvraz, 1986; Olivier & Sorensen, 1990). Such polydispersity often occurs in systems which have aggregated. The cumulant ratio μ_2/μ_1^2 is also a measure of polydispersity and was very large, $\mu_2/\mu_1^2 \simeq 0.4$–0.6, for these samples when $x > 2$. Similarly, the CONTIN fit showed a broad distribution for these samples. Such samples were not used in our reported size determination.

Careful preparation of samples led to the proper q^2 dependence and reasonable cumulant ratios of $\mu_2/\mu_1^2 < 0.1$. Both the one- and two-cumulant fits yielded consistent values, but the two-cumulant fit gave better fits using the chi-squared technique and run-to-run consistency of μ_1, and hence its values were used for size determination. The viscosities of the buffers were determined at 22 °C using a Poiseuille flow viscometer (average of 10 measurements). All QELS measurements were made within 1.8 °C of 22 °C; η values were corrected to values corresponding to the measured temperatures of QELS measurements by multiplying them by the change in viscosity of water for the temperature differences. At 22°, η values of 0.981, 0.986, and 0.976 centipoise were found for 50 mM Na MOPS(pH 7.4), 50 mM sodium phosphate (pH 7.4), and 50 mM potassium phosphate (pH 7.4), respectively.

Each data point in Figures 2–5 represents an average of 4–10 τ_c values that were derived from distinct data sets like the one shown in Figure 1.

Sedimentation Velocity Studies. Sedimentation velocity studies were conducted in double-sector cells with Beckman Spinco Model E Ultracentrifuges equipped to observe the sedimentation boundary either by schlieren optics (protein concentrations 2–4 mg/mL) or by UV scanning detection at 280 nm (protein concentration 0.3–1 mg/mL). Schlieren boundaries were photographed and read with a 2-D micro-comparator and plotting, and least-squares analyses of slopes of ln R vs time plot gave S values with ±0.1 S or better precision (e.g., data in Figure 4 series A show 3 of 15 frames; the slope for ln R vs time plot had ρ^2 value of 0.99989 and standard error coefficient of 3.68×10^{-8}). The largest error is the systematic error introduced in the calibration and any slight subsequent drift of the electronic temperature control. To minimize temperature gradients, all runs were made at the temperature measured for the room-temperature equilibrated rotor. Output in UV scanning runs was directly to a PC equipped with Microstar Laboratories 12004 data acquisition processor. Data were processed with a convoluting moving window function as described by Savitzky and Gulay (1964).

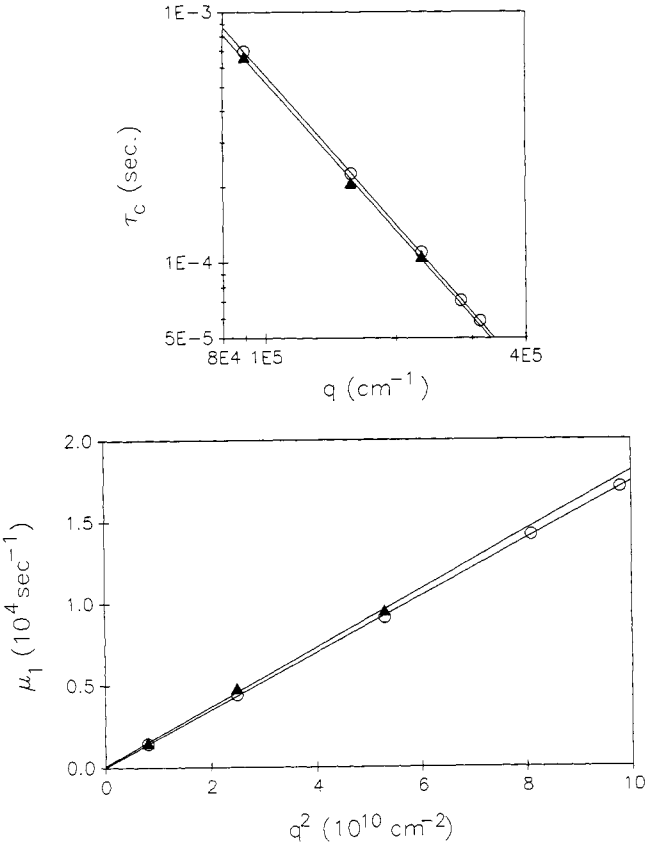

FIGURE 2: Light scattering by the bovine heart pyruvate dehydrogenase complex. Panel a (top) shows relationship between the correlation time, τ_c, and the scattering wave vector, q, for the heart pyruvate dehydrogenase complex before (○) and after (▲) gel filtration, which was conducted as described under Experimental Procedures. Measurements were made at angles of 90°, 58°, and 32° for each sample and additionally at 148° and 122° for the pre-gel-filtration sample. QELS measurements were at 23.4 °C for the pre-gel-filtration sample and at 21.7 °C for the post gel filtration. Least-square lines calculated by Sigma Plot program gave slopes of 1.99 and 1.97, respectively. Panel b (bottom) shows a plot of the cumulant μ_1 versus q^2 for heart pyruvate dehydrogenase complex before (○) and after (▲) gel filtration. The slope/2 equals D and allows an r_H value to be determined on the basis of measurements at all angles. D values were 8.7×10^{-8} cm^2/s (○) and 9.0×10^{-8} cm^2/s (▲). Slopes were determined as least squares values by Sigma Plot program.

The data were recursively fit with a cubic function generating both smoothed and first-derivative profiles.

RESULTS

Diameter of Non-Gel-Filtered Bovine Heart Pyruvate Dehydrogenase Complex. QELS measurements at angles of 148°, 122°, and 90° gave hydrodynamic radii r_H ranging from 26.0 to 26.2 nm indicating this apparently symmetric complex had a particle diameter of 52.2 nm. When measurements were made at lower angles (58° and 32°), slightly lower diameters of 51 nm were obtained. A log–log plot of τ_c versus q was linear and gave a least squares slope of 1.99, indicating that this was a well-behaved system (data not shown). Four to eight measurements made at two or three sample times were averaged for each angle used. A cumulant ratio for individual measurements was satisfactory. Thus the system appeared to be monodisperse or very nearly monodisperse. The particle diffusion coefficient based on the data at all the angles can be obtained from plotting μ_1 versus q^2 (Figure 2b). Equation 2 shows that the slope of this plot is

Table I: Effect of Dilution on QEL Measurements[a] of Gel-Filtered Bovine Kidney Pyruvate Dehydrogenase Complex

concentration complex (mg/mL)	θ	CONTIN fit[b] (r_H)	cumulant fit (r_H)
2.7	90°	24.0	24.0
2.7	32°	22.4	22.0
0.54	90°	24.3	24.6
0.54	32°	23.7	21.0
0.18	149°	24.6	25.0
0.18	123°	25.7	24.6
0.18	90°	24.8	24.7
0.18	55°	23.5	21.3
0.18	30°	24.6	18.5

[a] Measurements were made on fraction 26, which eluted just after the peak center from the gel filtration column. Data were acquired at 24.5 °C for 300 s using the ALV 5000 correlator. Other conditions were as in the legend to Figure 1; η at 24.5° for buffer was calculated to be 0.926 centipoise. [b] Provencher (1982).

$2D$. Once D is obtained, eq 3 yielded a particle diameter of 52.2 nm (Table I).

The quality of the above data indicated that little or no aggregate was present in the sample. However, some preparations of heart and kidney complex gave higher r_H values (27–31 nm), suggesting aggregation could influence the observed values. While aggregates were not detected in sedimentation velocity studies using the above sample of heart complex, a trace of stable dimer was detected in a sample of kidney complex that gave an r_H of ~30 nm and had a poorer cumulant ratio value and chi-squared fit for the net correlation function. These results and studies (below) with E2–X–K_cK_b subcomplex indicated that stable aggregates of complexes formed and could probably be removed by gel filtration chromatography. The effects of gel filtration on QELS-derived r_H measurements for the kidney complex are somewhat larger than we can explain on the basis of theoretical estimates[4] of the expected effects of aggregates detected in sedimentation velocity experiments. Additionally, unanticipated changes were also observed following fractionation of the bovine heart complex by gel filtration (below).

Gel-Filtered Complexes. Gel filtration chromatography was performed on the heart pyruvate dehydrogenase complex used above and on several samples of kidney complex that had given a range of r_H values. Using a 60-cm Sephacryl S400

[4] The z-averaged diffusion coefficient is given by

$$D_z = \sum_i n_i M_i^2 D_i \Big/ \sum_i n_i M_i^2$$

where n_i is the number density, M_i is the mass, and D_i is the diffusion coefficient of the ith species. The M_i^2 dependence comes from the fact that light scattered from small particles is proportional to M^2 (i.e., r^6 for spherical particles). To get a feel for how a small population of dimers would affect the measured D_z, we assume a system of monomers and dimers with concentration ratio of 10:1. The dimer diffusion coefficient should be bounded by the diffusion coefficient for a volume equivalent sphere with $R_2 = 2^{1/3}R_1$, hence $D_2 = 2^{-1/3}D_1$ and a sphere with a diameter equal to the length of two monomers, hence $R_2 = 2R_1$ and $D_2 = 2^{-1}D_1$. Under these conditions one finds D_z to be 6–15% smaller and hence the inferred r_H to be 6–15% larger, respectively, than the monomer r_H. The heart and kidney complexes yielded r_H values 5–25% larger before gel filtration than after. This very roughly implies ~10% dimers which would have been seen in the sedimentation runs. In fact, we could detect no aggregates in some sedimentation runs on complex that gave high values (e.g., Figure 4a). Furthermore, when ~10% dimers were seen in the E2–X–K_cK_b subcomplex, r_H could not be determined because of the q^3 dependence. Hence we conclude the sedimentation and QELS measurements are not consistent with regard to aggregate detection. We note, however, that lesser amounts of dimer below sedimentation detectability, say <5%, combined with even smaller amounts of trimers, quatramers, etc., might change r_H by 10% or more.

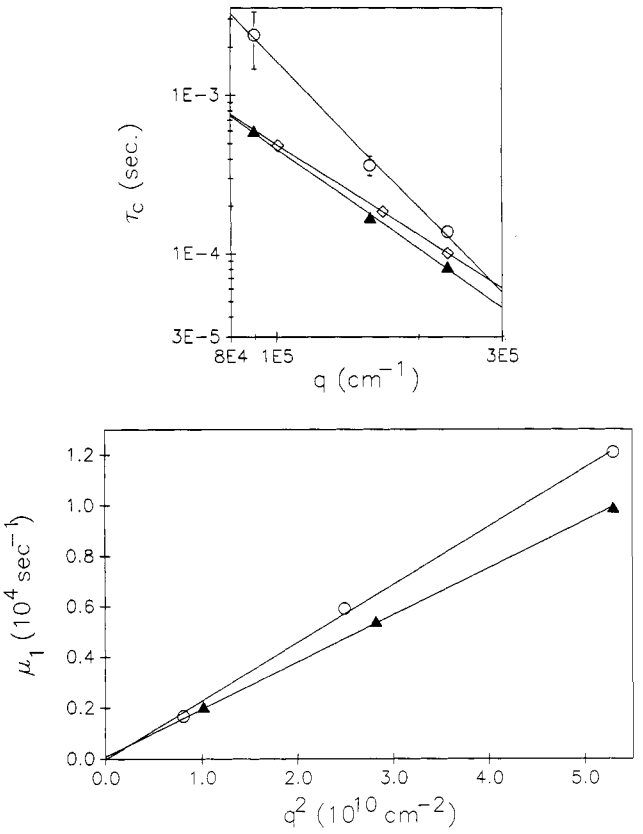

FIGURE 3: Light scattering by bovine kidney pyruvate dehydrogenase complex and kidney E2–X–K_cK_b subcomplex. Panel a (top) shows the relationship between changes in τ_c and q for the kidney E2–X–K_cK_b subcomplex before (O) and after (▲) gel filtration and for kidney pyruvate dehydrogenase complex after gel filtration (◇). Measurements were at angles of 90°, 58°, and 32° for the samples of subcomplex and at 90°, 62°, and 36° for the intact complex. QELS measurements on the E2–X–K_cK_b subcomplex were in 50 mM K_xPO_4 (pH 7.4) at 23.1 °C prior to gel filtration and in 50 mM Na_xPO_4 (pH 7.4) at 23.8 °C after gel filtration, and those on the intact kidney complex were in 50 mM Na MOPS (pH 7.4) at 23.2 °C. The gel-filtered samples gave slopes of 1.91 and 2.1 for complex and subcomplex, respectively, whereas the pre-gel-filtration sample of subcomplex gave a slope of ~3. Panel b (bottom) shows a plot of cumulant μ_1 versus q^2 for gel-filtered kidney pyruvate dehydrogenase complex (▲) and for the E2–X–K_cK_b subcomplex (O). The slopes/2 gave D values of 9.3×10^{-8} cm^2/sec and 11.5×10^{-8} cm^2/sec for the complex and subcomplex, respectively.

column, small amounts of kidney complex eluted as a leading shoulder on the major peak. To avoid interferences from this fraction, samples used for the initial measurements (cf. below) were collected from the second half of the major peak. At θ = 90° an r_H of 24.3 nm for the heart complex was determined with excellent agreement of data and fits of the correlation function. Three measurements at 10-μs sample time agreed within less than 1%. Lower angles, e.g., 32°, gave a slightly lower r_H value of 23.2 nm, and the slope of the log τ_c vs log q plot (Figure 2a) was 1.97. From the least-squares slope of the μ_1 vs q^2 plot shown in Figure 2b, an r_H of 24.3 nm was obtained. It should be noted that the data for the pre-gel-filtration heart complex and post-gel-filtration heart complex have considerable overlap in Figure 2, panels a and b, because the small increase in diffusion rate for the gel-filtered complex was compensated by the lower temperature (21.7 versus 23.4 °C) for QELS measurements on gel-filtered complex.

Prior to gel filtration, diameters determined at θ = 90° for various preparations of kidney complex ranged from 51.5 to 61 nm. Figure 3 panels a (◇) and b (O) show data for a gel-filtered kidney complex which had r_H of 24.4 nm indicating a particle diameter of 48.8 nm from measurements at 90°. Again, somewhat lower values were obtained at lower angles, and the slope of μ_1 versus q^2 plot gave a particle diameter of 48.0 nm. Because gel filtration had the largest effect on the r_H measurements for kidney complex and because of a concern (cf. Discussion) that reversible aggregation may occur, further studies were conducted on the kidney complex.

Analysis through the Gel Filtration Peak and Evaluation of Reversible Aggregation. A preparation of kidney complex that initially gave an r_H >29 nm in QELS measurements was passed through the gel filtration column, and QELS measurements were made on fractions throughout the peak. Complex eluting at the leading edge of the gel filtration peak gave an r_H >30 nm at θ = 90° and a poorer cumulant ratio than the starting material. Surprisingly, stable aggregates were not detected in a sedimentation velocity analysis of this sample (Figure 4, A series).[4] While complex from the trailing edge of the peak gave an r_H of ~25 nm, it had essentially the same $S_{20,w}$ (70.2 vs 70.3; protein concentrations of 4.0 and 3.9 mg/mL, respectively) as complex from the peak-front from the Sephacryl 400 column. In contrast to those results, another preparation of kidney PDC, which prior to the gel filtration step gave an r_H only slightly above 26 nm, gave uniform r_H values in QELS measurements made on samples from throughout the gel filtration peak of 24–25 nm for measurements at θ = 90°. A sample of complex from a fraction collected in the middle of the gel filtration peak gave $S_{20,w}$ of 71.5 at 2.7 mg/mL (cf. schlieren pattern, Figure 4, series B) and a rough $S^\circ_{20,w}$ of 73.[5] This sample was analyzed further.

Because of the possibility of reversible aggregation yielding a larger than correct size (and the broadness of the sedimentation boundaries, cf. Discussion), we performed QELS measurements on the preparation that gave uniform values in the gel filtration peak at 5- and 15-fold lower concentration (i.e., 0.54 and 0.18 mg/mL). As shown in Table I, there was no significant change in r_H determined at 90° for each of these concentration; and for the sample at 0.18 mg/mL for angles from 55° to 149°, r_H values based on the CONTIN fit (Provencher, 1982) were constant and within experimental error of r_H values obtained at 90° with the concentrated sample. Thus, these data strongly indicate that reversible aggregation is not contributing to the r_H values determined in the light scattering experiments. Three independent experiments on different preparations of bovine kidney complex gave average r_H values determined at 90° by multiple QELS measurements that ranged from 24.1 to 24.4 nm. Despite this high reproducibility, other experimental considerations (temperature measurements, angle measurements, possible effects of trace levels of aggregates) limit the accuracy for each experiment to ±1 nm.

Data for various measurements of the heart and kidney complexes are summarized in Table II. An important conclusion is that the kidney complex has a particle size equivalent to that of the heart complex (cf. Discussion) even though the kidney complex has only about two-thirds as much E1 component as the heart complex (i.e., its M_r ~ 1.5×10^6 lower) (Linn et al., 1972; Reed, 1974).

[5] The procedure (Roche & Cate, 1976) used for purifying the bovine kidney complex generally yields preparations with $S^\circ_{20,w}$ to 74 S for different preparations; plots of $S_{20,w}$ vs protein concentration have given slopes close to 0.7 S per mg/mL for the various preparations of kidney complex. A slightly lower $S^\circ_{20,w}$ value was obtained for kidney complex prepared by the early procedure of Linn et al. (1972). This probably reflects small losses of E1 and E3 in the earlier procedure which gave a product with a lower specific activity.

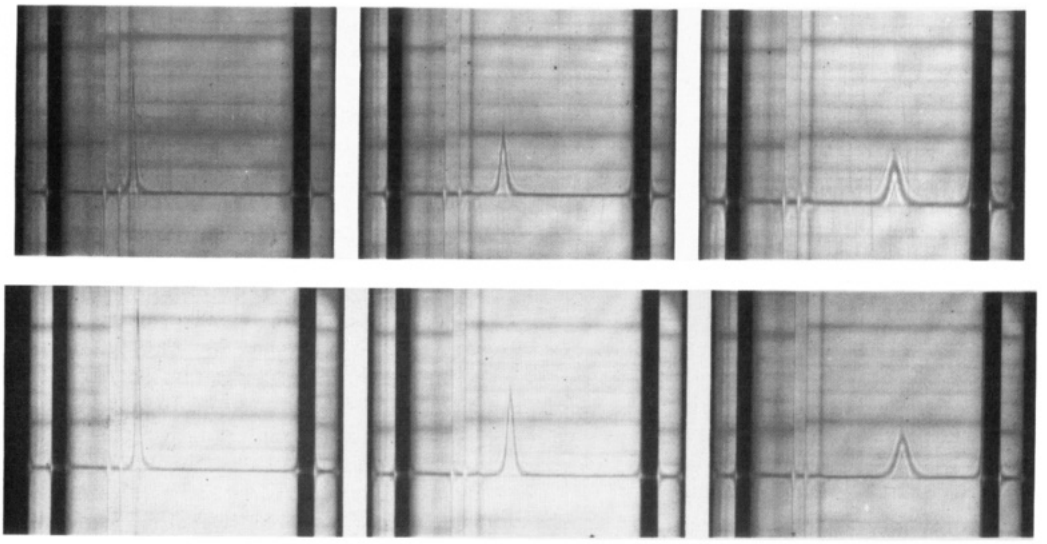

FIGURE 4: Sedimentation velocity patterns for gel-filtered bovine kidney complex. Panel a (top) shows the pattern for complex (4.0 mg/mL) eluting at the leading edge of the gel filtration peak, and panel b (bottom) shows the pattern for complex (2.7 mg/mL) eluting in a different experiment from the middle of the gel filtration peak. Experiments were conducted at 22 000 rpm at 23.4 °C (panel a) and at 24.3 °C (panel b). Fifteen frames were taken at 4-min intervals, and those at 4, 16, 36 min are shown. The bar angle was 60° throughout the run shown in panel a and for the first two frames of panel b but was changed to 50° in the final frame of panel b. Other considerations are described under Experimental Procedures.

Table II: Summary of Measured Diameters[a] of Enzyme Complexes and Slope Log τ_c vs Log q Plot

sample	diameter (nm) from scattering angle 90°	diameter (nm) from q^2 vs μ_1 plot	slope log τ_c vs log q
heart PDC	51.9	52.2	1.99
heart PDC gel filtered	48.7	48.6	1.97
kidney PDC gel filtered	48.8	48.0	1.91
E2–X–K_cK_b gel filtered	40.3	40.1	2.11

[a] Diameters are based on data from Figures 2 and 3. For the intact pyruvate dehydrogenase complexes that underwent gel filtration, the precision of these measurements is ±1 nm and the reproducibility between experiments is even better. However, considering all the contributing measurements (η, temperature, θ, and QELS data) the accuracy is only ±2 nm. For the E2–X–K_cK_b subcomplex, the accuracy for the measured diameter is somewhat lower (±3 nm) due to a greater problem with aggregation, but the precision and reproducibility for measurements at $\theta = 90°$ was again ±1 nm.

Aggregates of E2–X–K_cK_b Subcomplex and Reconstituted Complex Detected by QELS and Velocity Centrifugation. Initial measurements of the E2–X–K_cK_b subcomplex gave log τ_c versus log q plots with a slope of ~3.0 (Figure 3a) and values varied with sample time used for data accumulation. A slope of 3.0 is characteristic of a polydisperse system and suggested extensive aggregation. Velocity centrifugation (Figure 5, panel A) detected primarily monomer ($S_{20,w}$ = 34.7) but also detected low amounts of subcomplex that appeared to be a dimer ($S_{20,w} \simeq 51.5$) and very low levels of molecules that were probably trimers. The presence of lower levels of larger aggregates are suggested by the slope of 3 in the log τ_c versus log q plot. Since light scattering increases with the 6th power of the radius, even very low levels of such aggregates would have a significant impact on the scattered light. The pronounced effect of aggregates appears greater than we can explain on the basis of the levels of apparent dimer and trimer forms of the subcomplex detected by sedimentation velocity.[4]

The use of a wide variety and range of concentrations of chaotropic agents (LiCl, urea, nonionic detergents, with or without disulfide reducing conditions) failed to remove aggregates. When the aggregated E2–X–K_cK_b was used to form reconstituted complex (25 E1 tetramers and 10 E3 dimers per E2–X–K_cK_b subcomplex), both light scattering and sedimentation velocity studies (Figure 5, panel B) determined that aggregation persisted and gave $S_{20,w}$ values of ~61.4 and ~88.9.

Diameters of E2–X–K_cK_b Monomers. E2–X–K_cK_b monomers were prepared as described under Experimental Procedures by gel filtration using Sephacryl S-400 column. QELS measurements were made immediately following chromatography and remained constant over several hours. A hydrodynamic r_H of 20.2 ± 0.4 nm was obtained as the average of seven measurements at an angle of 90°. Good chi-squared values were found for the fit of the intensity autocorrelation function. A plot of μ_1 vs q^2 gave a particle diameter of 40.1 [Figure 3b(▲)]. Thus there was a remarkable transformation in the data following gel filtration. The radius determined at an angle of 32° was slightly higher than those at 90° and 58°. This may reflect a trace of residual aggregate in the sample and cause the slope of log τ_c vs log q to increase from 2 (when only 90° and 58° measurements were considered) to 2.1 [Figure 3a(▲)].

On the basis of these data, we estimate the average hydrodynamic r_H determined at 90° would be no more than 1.5-nm high as a consequence of scattering from trace aggregates indicating a hydrodynamic diameter of 37–41 nm for the E2–X–K_cK_b subcomplex. Even the lower end of this range is larger than the diameter suggested in previous electron microscopy studies (Bleile et al., 1981; Oliver & Reed, 1982), and our measurement constitutes the first direct measurement of the hydrodynamic diameter of untreated particles in solution. Easom et al. (1989) using an indirect, electrophoretic technique estimated a diameter of chemically cross-linked subcomplex to be 37.6 nm. That overlaps with the bottom end of the range for our estimate (cf. Discussion). Considering the extremely small volume that outer domains of E2 components are occupying, we must emphasize that the estimated hydrodynamic size reflects the dynamic effect of those outer domains on particle diffusion and does not constitute a limiting particle diameter (cf. Discussion).

Measurements on the Isolated Lipoyl Domain ($E2_L$) of Transacetylase Subunits. As in the case of E2–X–K_cK_b

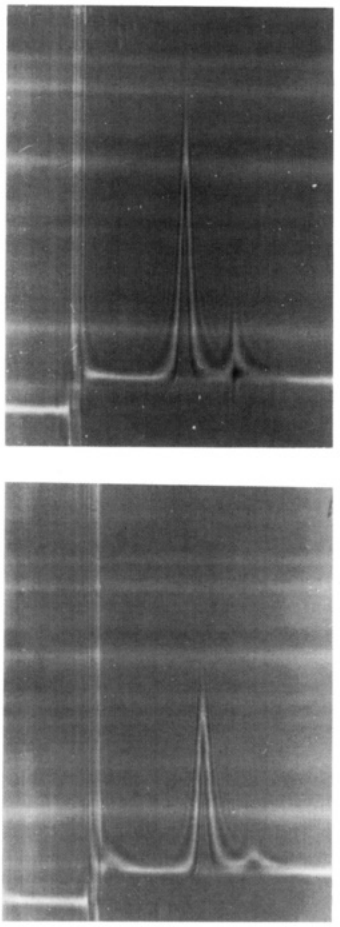

FIGURE 5: Sedimentation velocity pattern for E2–X–K_cK_b subcomplex (panel a, top) and reconstituted complex (panel b, bottom) prepared from this sample of subcomplex. Experiments were conducted at 30 000 rpm and on E2–X–K_cK_b subcomplex at 3.2 mg/mL at 23.0 °C and on reconstituted complex at 22.7 °C in 50 mM K_xPO_4 buffer (pH 7.4) with schlieren pattern recorded at a bar angle of 50°. The reconstituted complex was a mixture of 1.0 mg of E2–X–K_cK_b plus 1.0 mg of E1 of component and 0.4 mg of E3 component in 0.35 mL. Low levels of free E3 and E1 contribute to the pattern in the area of the meniscus in panel b.

subcomplex, the isolated $E2_L$ fragment gave a log τ_c versus log q plot with a slope of 3. Indeed τ_c values were larger than with the intact subcomplex. Surprisingly, sedimentation velocity studies detected only one peak with a very low S value of 1.3, but the boundary was sharper than would normally be expected for such a slowly sedimenting structure. The latter observation is consistent with the high frictional ratio (f/f_o = 1.9) reported by Bleile et al. (1981) for the slightly smaller tryptic fragment.

Following gel filtration chromatography on a Sephacryl S-300 column, measurements made at 90° were consistent over a 7-h period (indicating that aggregates did not rapidly occur). A hydrodynamic size of 10 ± 2.0 nm was estimated. The measurement could not be made more precise because of the relatively low scattering intensity due to the small size and low concentration (0.5 mg/mL) of this extended, 28-kDa molecule. It should be noted that the NH_2-terminal $E2_L$ fragment encompasses the two lipoyl domains and the following hinge region but does not include the E1-binding domain and the hinge region connecting that domain to the inner domain. Those parts of E2 are also part of its flexible outer structures. While lacking this 5-kDa portion of the outer domain and the hinge region connecting it to the inner domain (see Discussion), it is interesting to note that a contribution of even 9 nm on either side of inner domain of 22.5 nm gives a value of 41.5, nm which is close to our measurement of the size of E2–X–K_cK_b subcomplex.

DISCUSSION

Active site coupling that occurs in α-keto acid dehydrogenase complexes requires movement of lipoyl domains between at least three active sites and probably also involves interlipoyl transfer of acetyl groups and reducing equivalents. In the mammalian pyruvate dehydrogenase complex, the kinase and phosphatase components are also associated with the lipoyl domain region (Rahmatullah et al., 1990; Li et al., 1992; Rahmatullah et al., 1988) and function in the interconversion of the E1 component that is bound to B domain of E2. Those associations of the regulatory enzymes and their E1 substrate with the E2 core greatly enhance kinase (~5-fold) and phosphatase activity (~10-fold). Both the reactions of the complex and these regulatory processes which involve one regulatory enzyme acting on many E1 involve considerable dynamic movement of domains and components. The capacity for such movement depends on how open (solvent filled) an area is the portion of the complex exterior to the dodecahedron-shaped inner core structure formed by E2's inner domain. Danson et al. (1979) presented evidence that the *E. coli* complex retained a high level of solvent. The present work supports that conclusion for the mammalian complex.

With gel-filtered bovine kidney or more massive bovine heart complexes, r_H values of 24.1 ± 0.3 nm and 24.3 ± 0.6 nm, respectively, were found which agree with results using ice-imbedded electron microscopy (Wagenknecht et al., 1991b) but are 9% larger than radii from negatively stained images (Oliver & Reed, 1982) or from 2-D agarose gel electrophoresis (Easom et al., 1989). As in the case of studies on the *E. coli* pyruvate and α-ketoglutarate dehydrogenase complexes, ice-imbedded microscopy technique has consistently detected gaps between the inner domain and the components bound to the outer domains of the mammalian E2 (Wagenknecht et al., 1988, 1991a). While gaps are also detected in many negatively stained images (Oliver & Reed, 1982), the smaller diameters and/or loss of gaps in many images may have resulted from drying the samples on micrograph grids. Thus, the good agreement between our measurements in solution of the diameters of these nearly spherical intact complexes and those determined by the ice-imbedded electron microscopy indicate these measurements yield a consistant and accurate size determination.

In quasielastic light scattering and sedimentation velocity studies on the *E. coli* pyruvate dehydrogenase complex (Danson, et al. 1979), there were problems with the presence of species smaller and larger than the dominant one that did not allow the data to be analyzed as a monodisperse system. Nevertheless, the average values were corrected on the basis of the levels of the larger and smaller species observed in sedimentation velocity runs, and a particle radius for this octahedral-based system of 23.6–23.9 nm was found (Stokes radius of 23.9 nm was reported; r_H calculated from their data is 23.6 nm). In contrast, we have observed single boundaries for intact mammalian complex in sedimentation velocity runs; and, following gel filtration, we have obtained light scattering data that supported analysis by correlation functions for a monodisperse system. We cannot explain the marked change to a monodisperse system following gel filtration based on changes in sedimentation velocity patterns. Possibly large aggregates are removed but we would note that the microfuge treatment (cf. Experimental Procedures) should have removed very large particles.

As observed with *E. coli* complex (Gilbert & Gilbert, 1980; Schmitt & Cohen, 1980), boundaries for the bovine heart and kidney complexes are somewhat broader than would be expected if there were no molecular heterogeneity. Our data on r_H values strongly indicate that broadening is due to variation in the stoichiometry of components rather than a reversible association. We observed a constant r_H over a 15-fold concentration range with the kidney complex and no time-dependent variation in r_H before or after dilution. This is further supported by the agreement, within experimental error, in the sizes of the heart complex ($M_r \simeq 9 \times 10^6$) and the kidney complex ($M_r \simeq 7.5 \times 10^6$). The average stoichiometry for bound E1 is significantly lower for the kidney complex, but it can bind more E1 (Wu & Reed, 1984).

Even in the more massive heart complex, less than 20% of the volume between the inner core (diameter 22.5 nm) and the outer diameter (≥48 nm) is occupied by protein.[6] Thus our data indicate that a high level of solvent is entrained within the particle diameter of these complexes, which would seem to explain why these nearly spherical complexes have such high frictional coefficients ($f/f_0 > 1.8$).

As indicated above, the exterior multidomain segments of the E2 subunits have a central structural and mechanistic role in these multienzyme systems. Perham's laboratory (Texter et al., 1988; Perham & Packman, 1989) used ^{1}H NMR to demonstrate the high mobility of the hinge portions of the outer domains of the transacetylase component from bacterial sources. The molecular mass and distribution of the various domains of transacetylase subunits from several sources, including the human enzyme (Coppel et al., 1988; Thekkumkara et al., 1988), have been delineated from the amino acid sequences deduced from nucleotide sequences of cDNA clones of transacetylase components. The domain structures consist of one to three lipoyl domains (depending on the source), invariably followed by a subunit binding domain, and then an inner domain with connecting hinge regions between these domains [cf. reviews: Roche and Patel (1989), Reed and Hackert (1990), Patel and Roche (1990), and Perham (1991)]. Detailed structures of the globular domains are beginning to emerge. Besides the truncated inner domain structure of the *A. vinelandii* (Mattevic et al., 1992; cf. the introduction), the 3-D structure of the 5-kDa domain that binds the E3 component has been determined for the dihydrolipoamide succinyltransferase component of *E. coli* α-ketoglutarate dehydrogenase complex (Robien et al., 1992). The relationship between this domain and a related domain in mammalian E2 that binds the E1 component and a distantly related domain of protein X that binds E3 component will be of great interest.

Because of the central role of these exterior multidomain structures of E2, their high mobility, and the large frictional coefficient of both the intact E2 core and the isolated outer domains, it is of great interest to define the molecular dimensions of the outer domains in the assembled subcomplex. The elegant electron micrograph studies of Reed and Oliver (1968, 1982) indicated that the diameter of the rigid inner core dodecahedron structure formed by the inner domain of the bovine heart dihydrolipoyl transacetylase subunits was 21 nm. More recently, ice-imbedded electron microscopy found a somewhat larger diameter of 22.5 nm for the fully hydrated inner core (Wagenknecht et al., 1991b). Using 2-D agarose electrophoresis, Easom et al. (1989) estimated that the entire subcomplex structure had a particle diameter of 37.6 nm. Their core particles were cross-linked with glutaraldehyde. Our QELS measurements at $\theta = 90°$ should have the greatest accuracy, and the average of several measurements indicate a hydrodynamic particle diameter of 40.4 nm. The lack of cross-linking in our studies may allow the highly anionic outer lipoyl domains to extend out from the inner domain in a more uniform manner and for somewhat greater distances.

It is very important to recognize that even within the radial volume from the inner core (starting at 11.2 nm) to the hydrodynamic r_H values for the subcomplex of ~20 nm and for the whole complex of ~24.3 nm, that E2 oligomer's 60 35-kDa outer domain structures would occupy about 9% and 5% of those volumes, respectively. Thus, the observed hydrodynamic effect is very large and probably involves the flexing between positions within these dimensions to positions well beyond a 20-nm radius. Considering the large number of amino acids (>120) in the three linker regions between the three globular outer domains, a radial reach to 25 nm could be easily achieved and seems likely on the basis of the following considerations. Besides being highly mobile structures, Perham (1991) suggests that the high alanine and proline content of the hinge regions contributes to stiffness that would help to extend and keep the globular domains separated. Additionally, the lipoyl domains of mammalian E2 are very anionic and would be expected to repel each other. Finally, in work in preparation, cryoelectron microscopy evidence has been obtained that demonstrates the inner of the two lipoyl domains of the mammalian E2 is randomly distributed in particles of the E2–X–K_cK_b subcomplex within a diameter of about 52 nm.[7] A more regular or limited distribution may exist when the E1 and E3 components are bound.

It seems unlikely that either the ~6 protein X subunits or the ~2 kinase dimers contribute significantly to the measured hydrodynamic diameter. The inner domain of protein X is tightly associated with the inner domain of E2 subunits, and it has a smaller outer domain than E2 subunits (Rahmatullah et al., 1989a). The low stoichiometry of one to two kinase subunits per subcomplex would minimize the contribution of the kinase to the measured dimensions. The extended structure of the outer domain region is supported by our measurement of 10 ± 2 nm of the hydrodynamic diameter of $E2_L$ (which constitutes ~28 kDa of the 35 kDa of the outer domain structure of E2 subunits). Our inability to prepare this fragment in a concentrated form without aggregation limited the precision of the latter measurement.

In conclusion, previous work [e.g., Reed (1974)] indicated that the bovine kidney and heart complexes have the same organization. Our data are consistent with that and further indicate about 10 more E1 tetramers can be bound in the heart complex without expansion of the particle diameter. We have also detected a large effect of the of E2 subunits on the hydrodynamic properties of the E2–X–K_cK_b subcomplex which lacks the E1 and E3 components. Considering the very small volume occupied by these exterior, multidomain structures, we suggest that, at any instant, at least a small portion

[6] This calculation assumes per heart complex that each of the 60 outer domains of E2 have a molecular mass of ~35 kDa, each of the 30 E1 tetramers have a molecular mass of 154 kDa, each of the six E3 dimers have a molecular mass of 102 kDa, and each of two kinase dimers have molecular mass of 90 kDa; and it further assumes a specific volume for all protein of 0.74 mL/g. The measured value of 22.5 nm for the icosahedral inner core of E2 reported by Wagenknecht et al. (1991b) is now supported by a reconstruction made from further cryoelectron microscopy data that has resolution to 22 Å (V. V. P. Prasad, T. Wagenknecht, and T. E. Roche, manuscript in preparation).

[7] Wagenknecht and Roche (unpublished results). In part, this work involves locating the position of the inner lipoyl domain by increasing its mass through binding a F_{ab} fragment prepared from a highly specific monoclonal antibody.

of these domains range radially well beyond 20 nm to cause the diffusion rate of these particles to be that of a structure with an r_H of about 20 nm measured for the subcomplex. Indeed, it is likely that these reach beyond radial distance of 24.4 nm measured for the entire complex. Thus these outer E2 structures create drag like a swarm of randomly oriented cilia extending from an inner nearly spherical structure.

ACKNOWLEDGMENT

We thank Dave Manning for his help in conducting and analyzing sedimentation velocity experiments. We also thank Gary A. Radke for his skilled technical help and Connie Schmidt for secretarial assistance.

REFERENCES

Berne, B. J., & Pecora A. (1976) *Dynamic Light Scattering*, Wiley Interscience, New York.
Bleile, D. M., Hackert, M. L., Pettit, F. H., & Reed, L. J. (1981) *J. Biol. Chem. 256*, 514–519.
Bloomfield, V. A. (1985) in *Dynamic Light Scattering* (R. Pecora, Ed.) pp 363–416, Plenum, New York.
Coppel, R. L., McNerlage, L. J., Surh, C. D., Van de Water, J., Spithill, T. W., Whittingham, S., & Gershwin, M. E. (1988) *Proc. Natl. Acad. Sci. U.S.A. 85*, 7317–7321.
Danson, M. J., Hile, G., Johnson, P., & Perham, R. H. (1979) *J. Mol. Biol. 129* 603–617.
Easom, R. A., DeBuysere, M. S., Olson, M. S., & Serwer, P. (1989) *Proteins 5*, 224–232.
Gilbert, G. A., & Gilbert, L. M. (1980) *J. Mol. Biol. 144*, 405–488.
Jilka, J. M., Rahmatullah, M., Kazemi, M., & Roche, T. E. (1986) *J. Biol. Chem. 261*, 1858–1867.
Li, L., Radke, G. A., Ono, K., & Roche, T. E. (1992) *Arch. Biochem. Biophys. 296*, 497–504.
Linn, T. C., Pelley, J. W., Pettit, F. H., Hucho, F., Randall, D. D., & Reed, L. J. (1972) *Arch. Biochem. Biophys. 148*, 327–342.
Martin, J. E., & Leyvraz, F. (1986) *Phys. Rev. A 34*, 2346–2353.
Mattevi, A., Obmolova, G., Schulz, E., Kalk, K. H., Westpha, A. H., deKok, A., & Hol, W. G. J. (1992) *Science 225*, 1544–1550.
Oliver, R. M., & Reed, L. J. (1982) in *Electron Microscopy of Proteins* (Harris, R., Ed.) Vol. 2, pp 1–48, Academic Press, London.
Olivier, B. J., & Sorensen, C. M. (1990) *Phys. Rev. A 41*, 2093–2100.
Patel, M. S., & Roche, T. E. (1990) *FASEB J. 4*, 3224–3233.
Perham, R. N., & Packman, L. C. (1989) *Ann. N.Y. Acad. Sci. 256*, 514–419.
Provencher, S. W. (1982) *Comp. Phys. Commun. 27*, 213–227 and 229–242.
Rahmatullah, M., Gopalakrishnan, S., Radke, G. A., & Roche, T. E. (1989a) *J. Biol. Chem. 264*, 1245–1251.
Rahmatullah, M., Gopalakrishnan, S., Andrews, P. C., Chang, C. L., Radke, G. A., & Roche, T. E. (1989b) *J. Biol. Chem. 264*, 2221–2227.
Rahmatullah, M., Radke, G. A., Andrews, P. C., & Roche, T. E. (1990) *J. Biol. Chem. 265*, 14512–14517.
Reed, L. J. (1974) *Acc. Chem. Res. 7*, 40–46.
Reed, L. J., & Oliver, R. M. (1968) *Brookhaven Symp. Biol. 21*, 397–412.
Reed, L. J., & Hackert, M. L. (1990) *J. Biol. Chem. 265*, 8971–8974.
Roche, T. E., & Cate, R. L. (1977) *Arch. Biochem. Biophys. 183*, 664–667.
Roche, T. E., & Patel, M. S. (Editors) (1989) α-Keto Acid Dehydrogenase Complexes: Organization, Regulation, and Biomedical Ramifications, *Ann. N.Y. Acad. Sci. 573*,
Schmitt, B., & Cohen, R. (1980) *Biochem. Biophys. Res. Commun. 93*, 709–712.
Thekkumkara, T. J., Ho, L., Wexler, I. D., Pons, G., Lui, T.-C., & Patel, M. S. (1988) *FEBS Lett. 240*, 450–48.
Texter, F. L., Radford, S. E., Lane, E. D., Perham, R. N., Miles, J. S., & Guest, J. R. (1988) *Biochemistry 27*, 289–296.
Wagenknecht, T., Grassucci, R., & Frank, J. (1988) *J. Mol. Biol. 199*, 137–147.
Wagenknecht, T., Grassucci, R., & Schaak, D. (1991a) *J. Biol. Chem. 265*, 22402–22408.
Wagenknecht, T., Grassucci, R., Radke, G. A., & Roche, T. E. (1991b) *J. Biol. Chem. 226*, 24650–24656.
Wu, T.-L., & Reed, L. J. (1984) *Biochemistry 23*, 221–226.